Deep-inelastic reactions of $^{16}O + {}^{48}Ti$ at 100 MeV

R. Ritzka, W. Dünnweber, A. Glaesner, W. Hering, H. Puchta, and W. Trautmann*
Sektion Physik, Universität München, 8046 Garching, Federal Republic of Germany
(Received 28 August 1984)

The particle-inclusive doubly differential cross section, $d^2\sigma/dE\,d\theta$, for ejectiles with atomic numbers $Z=4$ to 15 from 100 MeV $^{16}O + {}^{48}Ti$, was measured over a large angular range. From a semiclassical analysis of the angular distributions we obtain the mean values and the dispersion widths of the deflection angles and the contributions from orbiting around 180°. A mean prolate deformation with $\beta=0.37$ is derived from the most probable Q values in the fully damped processes at large angles. Using the surprisal technique, the shapes of the energy spectra are well reproduced by constrained phase-space distributions. If the measured correlation of the angular momentum transfer and the reaction Q value is taken into account, only the mean Q values of the quasielastic and of the deep-inelastic reaction component are required as constraints.

I. INTRODUCTION

The appearance of a deep-inelastic (DI) reaction component is documented for a large variety of heavy-ion systems,[1,2] mostly in the range of bombarding energies between 5 and 10 MeV/nucleon. Its main characteristics are the following: (i) a mean energy close to the mutual-interaction barrier in the exit channel, (ii) a broad mass distribution centered in the vicinity of the projectile, and (iii) a nonisotropic angular distribution $d\sigma/d\theta$. Most of the detailed studies have been performed with heavy projectiles ($A \geqq 40$), but a distinct DI component with features (i)—(iii) is also known to exist in light-heavy-ion-induced reactions ($A \leqq 20$).[3–9] In contrast to what is found with heavier projectiles, this component accounts only for a modest part ($\lesssim 10\%$) of the total reaction cross section. This indicates a localization in angular momentum space caused by the absorption of partial waves with $l \lesssim l_{\text{crit}}$. In the case of 100 MeV $^{16}O + {}^{48}Ti$, the critical angular momentum for fusion is calculated to be $l_{\text{crit}} = 41\hbar$, using the Bass model which well accounts for fusion cross sections in several neighboring systems.[10,11] In the sharp cutoff approximation, DI and quasielastic (QE) reactions share the range of partial waves between l_{crit} and the grazing value, $l_{\text{graz}} = 50\hbar$.

Since several particle-γ coincidence studies have been devoted to ^{16}O-induced DI reactions,[5,12–17] revealing various features of angular-momentum relaxation, we found it rewarding to revisit such a case and to investigate in some detail the particle-inclusive distribution in energy and angle. We have chosen the system $^{16}O + {}^{48}Ti$ at a bombarding energy of 100 MeV for which γ-ray multiplicities, angular correlations for discrete transitions, and circular polarizations are available.[13–15] The purpose of this paper is to discuss, in light of the information on the angular-momentum transfer, the following aspects of the doubly differential cross section $d^2\sigma/dE\,d\theta$:

(1) The forward-peaked angular distributions can be interpreted in terms of large fluctuations of the trajectories about mean deflection angles. In a semiclassical analysis, we deduce these mean angles and the widths of the angular dispersion from the slopes of the angular distributions and from the relative strengths of the near-side and far-side components, derived from the polarization data.[15] Quantal and classical dispersion are found to be of comparable importance in the present system (Sec. IV).

(2) The most probable exit-channel energies are divided into rotational and potential energies. The contribution of the rotational energy is rather important in a light system. It is calculated on the basis of the experimentally known angular-momentum transfer.[13,14] The deduced potential energy gives evidence of the dynamical deformation of the fragments (Sec. V).

(3) The shapes of the energy spectra are subjected to a surprisal analysis[18,19] which enables a comparison with equilibrium distributions in a constrained phase space. Using a level density which takes the measured Q-dependent angular-momentum transfer into account, only the mean Q values of the DI and of the QE reaction components are required as constraints. This procedure is considered as an alternative to the introduction of an additional constraint[19] imposed on the width of the distribution of exciton numbers. In view of the relaxed spin-vector distribution,[13,14] it is of interest whether the DI energy distribution about its mean is relaxed as well (Sec. VI).

These discussions are preceded by a description of the experimental details (Sec. II) and by a survey of the gross properties of the measured doubly differential cross section (Sec. III).

II. EXPERIMENTAL METHOD

A beam of 100-MeV $^{16}O^{8+}$, supplied by the Munich Tandem accelerator, was used to bombard a metallic ^{48}Ti target of 500 $\mu g/cm^2$ areal density and of 99.1% isotopical enrichment. The scattered heavy ions were detected with ΔE-E telescopes consisting of axial-field ionization chambers and 20-cm^2 Si surface-barrier counters. The telescope used at forward angles ($\theta_{\text{lab}} \leq 60°$) was filled

with a mixture of 90% argon and 10% methane at a pressure of 50 Torr, which was stabilized by means of a gas-flow control. The active length between the entrance foil of 280 $\mu g/cm^2$ Mylar, covered by 40 $\mu g/cm^2$ Al, and the Si counter, stopping particles at the rear end of the ionization chamber, was 6 cm. An anode ring at a voltage of + 100 V, mounted in the center of the gas tube, provided energy-loss (ΔE) signals which were in good approximation independent of the position of the ionization track because of the axial-field geometry. This rather compact detector was mounted inside the scattering chamber with a distance of 14 cm between the target and the entrance foil. An aperture defined an angular acceptance of $\pm 2°$. The atomic numbers of fragments up to $Z=15$ were clearly resolved (Fig. 1) with $\Delta Z/Z=0.04$ (FWHM) at count rates of up to 10 kHz of which typically 20% were due to ions heavier than α particles.

The measurements at angles larger than 60° (lab) were carried out with a thinner target (245 $\mu g/cm^2$) and lower gas pressure (25 Torr) in order to accommodate to the lower energies of the ejectiles in the laboratory frame. In these runs the target was tilted by 45° with respect to the beam axis so that the ejectiles were detected in reflection geometry.

An ionization chamber at a fixed angle of 45° monitored the yield from elastic scattering on a 0.4 $\mu g/cm^2$ tungsten admixture in the target material in order to normalize the relative cross sections at the different angles. The inelastic yield from the tungsten admixture is negligibly small. The absolute cross sections were determined to within $\pm 10\%$ by normalizing the yield per integrated current on the Faraday cup for the reaction under investigation, to the yield from Rutherford scattering on a pure gold target of known thickness at various forward angles.

The data were processed by a PDP 8/10 on-line system and analyzed off line by setting appropriate gates on the individual Z branches in the ΔE-E matrix (Fig. 1). The recording of protons and α particles was suppressed by setting an electronic threshold on the ΔE signals.

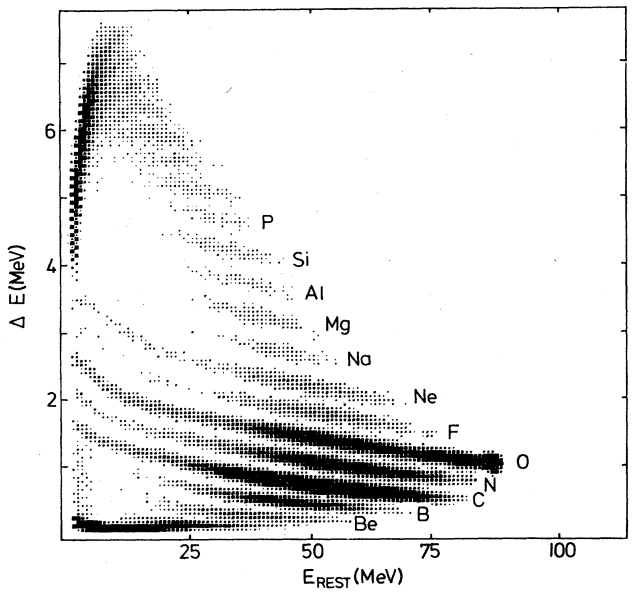

FIG. 1. Scatter plot of the (ΔE,E_{rest}) signals from a heavy-ion detector positioned at 30°. The area of the symbols is proportional to the number of events between 5 (smallest size) and 105 (largest size).

To derive the energies from the Si counter signals, values for the loss of energy in the target, in the entrance foil, and in the gas volume were adopted from the tables.[20] The positions of the elastic scattering peaks, observed at bombarding energies of 56.25 and 100 MeV at various angles with various targets, were used for the calibration and as a check of the adopted values of the energy loss. This calibration accounts in linear approximation for the small pulse-height defect in the Si counter.[21]

The energies and scattering angles of the ejectile were transformed into the center-of-mass system by assuming two-body kinematics. This is a reasonable approximation in the $Z=6$, 7, and 8 channels, where an upper limit of 15% is established for contributions from sequential decay of the ejectile or from fast breakup processes by the strength of the coincident γ transitions in the targetlike fragments.[13] This is consistent with a study of three-body processes in 100-MeV $^{16}O+^{58}Ni$ (Ref. 22). In the case of heavier ejectiles, sequential decay is probably more important and the resulting uncertainty is indicated where appropriate. Since the mass of the ejectile was not measured, the kinematic transformation was done for the most probable isotope of each element number, following the Q_{gg} systematics which was shown to work well for 100-MeV ^{16}O-induced reactions on other medium-mass target nuclei.[23] For $Z=6$ and 8, e.g., abundances of ^{12}C and ^{16}O of 85 and 75%, respectively, are predicted at the most probable DI Q values. In these cases a shift of the c.m. energy by about $+(-)0.5$ MeV would result from increasing (decreasing) the mass by one unit. The given energies and angles represent averages over the isotopic distributions of the ejectiles.

In order to correct for contributions from light-element impurities of the target, comparative runs were performed with a pure carbon target. The spectra obtained with the carbon target were normalized to the yield at $Q<-60$ MeV in the spectra obtained with the former target and subtracted from these. A common normalization was found for the $Z\leq 6$ channels, in agreement with the expectation that carbon is the dominant light contaminant. For larger Z, individual normalizations were required, indicating the presence of additional contaminations like, e.g., oxygen. In these cases the very small corrections rely on the assumption that the shapes of the spectra from the additional contaminants are similar to those from carbon. Except for $Z\leq 6$ at $Q<-40$ MeV and $\theta_{lab}<30°$, the corrections were smaller than 5% of the yield in the original spectra.

III. GROSS PROPERTIES OF THE DOUBLY DIFFERENTIAL CROSS SECTION

A comprehensive view of the doubly differential cross sections is obtained from contour plots (Wilczynski plots[24]) in the E_f-$\theta_{c.m.}$ plane (Fig. 2), where $E_f=E_i^{c.m.}+Q$ is the total kinetic energy of both fragments in the c.m. frame. The observed correlation of energy and angle is suggestive of the evolution of the system

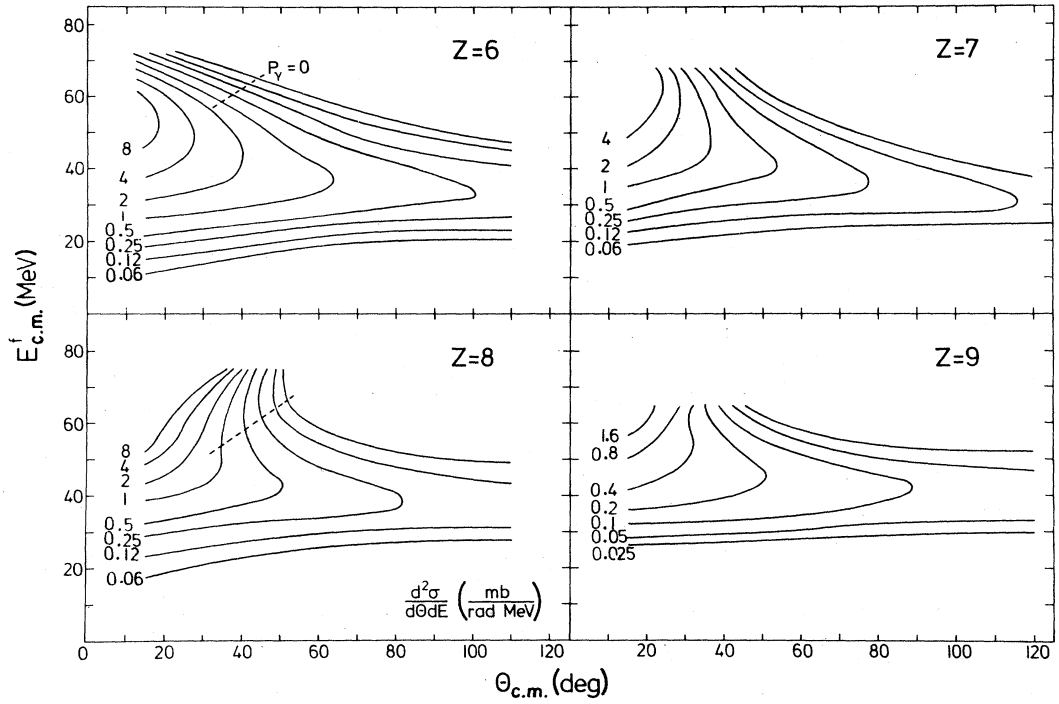

FIG. 2. Contour plots of the doubly differential cross section in the center-of-mass frame for different reaction channels. The dashed line indicates the locus (±2 MeV) of a vanishing γ-ray circular polarization, as determined in Ref. 15. The polarization is negative (positive) above (below) this line, corresponding to predominantly positive (negative) scattering angles.

with increasing interaction time—though not as clearly as in cases of heavier systems with a larger separation in energy between elastic scattering and full damping.[1,2] The ridge line from negative-angle scattering[15] at low E_f is rather flat at angles larger than 50° in all reaction channels, suggesting that a rather fast damping of energy has occurred in the range of smaller angles. Only in the $Z=8$ case is one guided by the contour plot to continue this ridge across 0° towards positive scattering angles in the QE region, as proposed by Wilczynski.[24] The contour plot for $Z=9$ is weakly suggestive of a similar evolution. However, a rather clear-cut division of these plots into regions of predominantly positive- or negative-angle scattering is provided by the γ-ray circular polarization data.[15] The borderline between these two regimes is indicated in Fig. 2 for the $Z=6$ and 8 cases which have the smallest statistical uncertainties. For all exit channels from $Z=5$ to 10, the ridge at low E_f is associated with a positive average polarization, corresponding to negative scattering angles.[15] Guided by this common behavior of the various reaction channels, we may operationally define the DI reaction component in the present system as being constituted by the ridges at low E_f.

The correlation between energy loss and scattering angle can be seen in more detail in Fig. 3 where the energy spectra for $Z=6$ and 8, the strongest reaction channels (see Fig. 1), are shown for different angles in the laboratory frame. A shift towards larger energy loss with increasing angle is observed in all cases with $Z \leq 10$, but it is most marked in the $Z=Z_{\text{projectile}}$ channel.

At 20°, which is close to the grazing angle, the oxygen

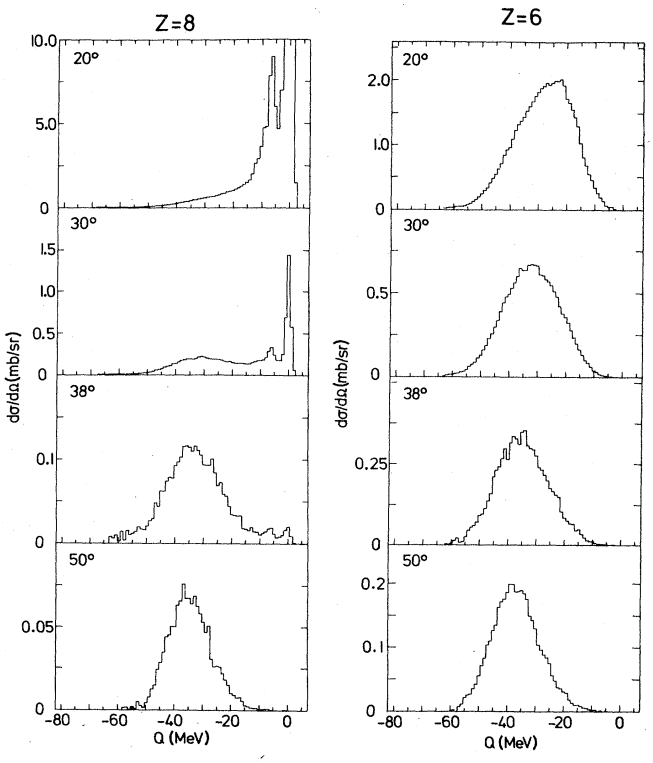

FIG. 3. Energy spectra of $Z=6$ and 8 ejectiles at different angles in the laboratory frame.

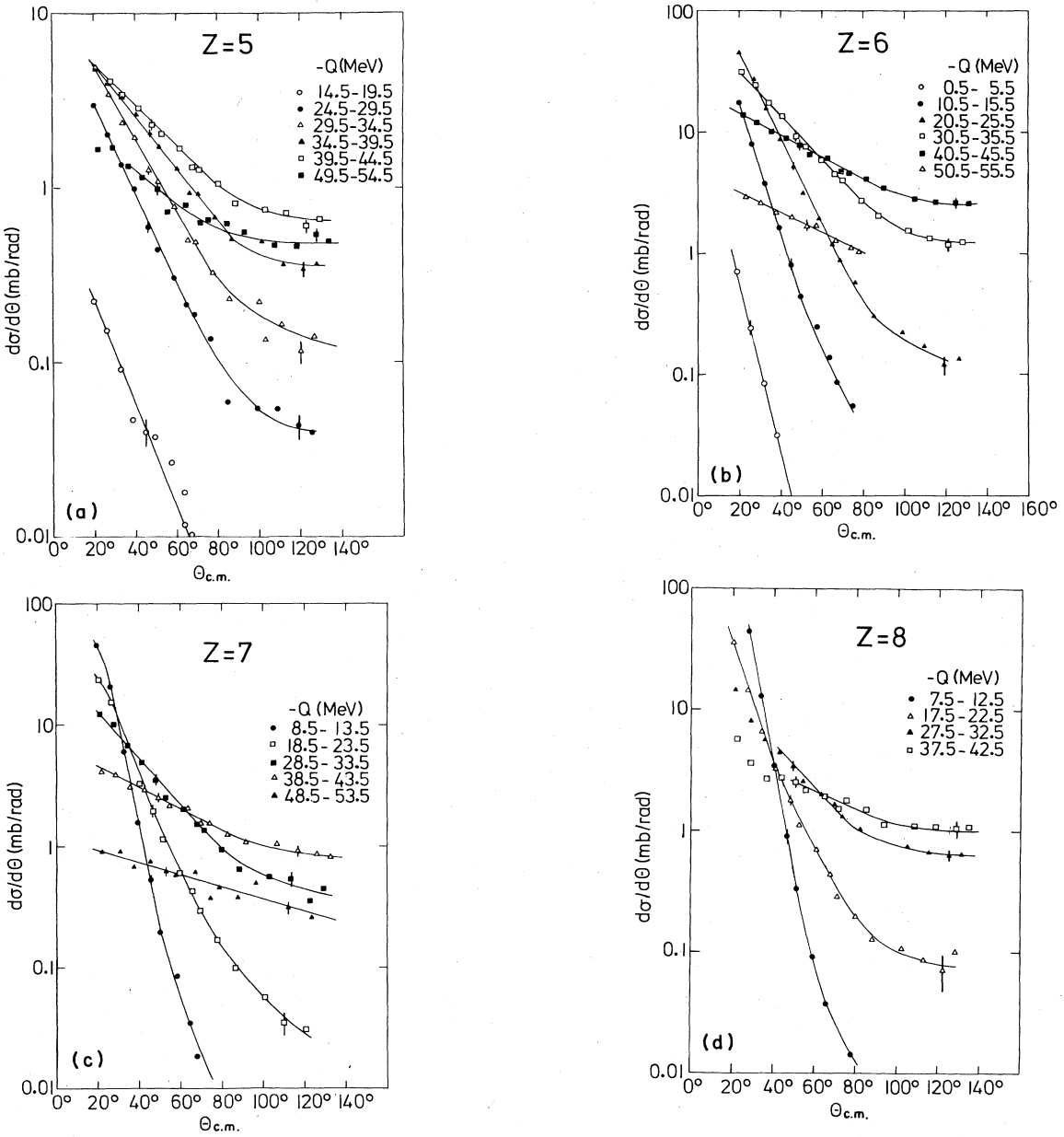

FIG. 4. (a)—(f) Differential cross sections in the center-of-mass frame for different reaction channels. These cross sections are the integrals over the energy in the given Q-value bins of 5 MeV width. Lines are drawn to guide the eye.

spectrum is dominated by the elastic peak and a shoulder in the QE region. In addition, a peak stands out at a position consistent with the excitation energy of the first 3^- state of ^{16}O, $E_x = 6.1$ MeV. The spectrum decreases monotonically with increasing inelasticity. At 30°, a smooth valley appears around $Q \approx -15$ MeV which is suggestive of two-component characteristics of the spectrum. With further increase of the angle, the intensity in the QE region drops out rapidly so that the bell shaped DI component becomes predominant at 50° and beyond.

In the carbon spectra a single broad bump is observed. The optimum Q value for a one-step α transfer expected from classical orbit matching with inclusion of the recoil effect,[14,25] $Q_{opt} = -23$ MeV, is separated by less than the full width at half maximum from the center of the bell-shaped distribution observed at $\theta_{lab} > 50°$. Therefore, a decomposition into QE and DI is not apparent in these spectra. However, the considerable change of their shape with angle, which is clearly seen in Fig. 3 by comparison of the spectra at 20° and 38°, has been taken as evidence for the presence of two components in the similar case of the (^{16}O,^{12}C) reaction on ^{58}Ni at 100 MeV (Ref. 26). The polarization data as well as the surprisal analysis (Sec. VI) substantiate such a decomposition.

Horizontal cuts of the Wilczynski plots are given by the angular distributions in Fig. 4. These differential cross

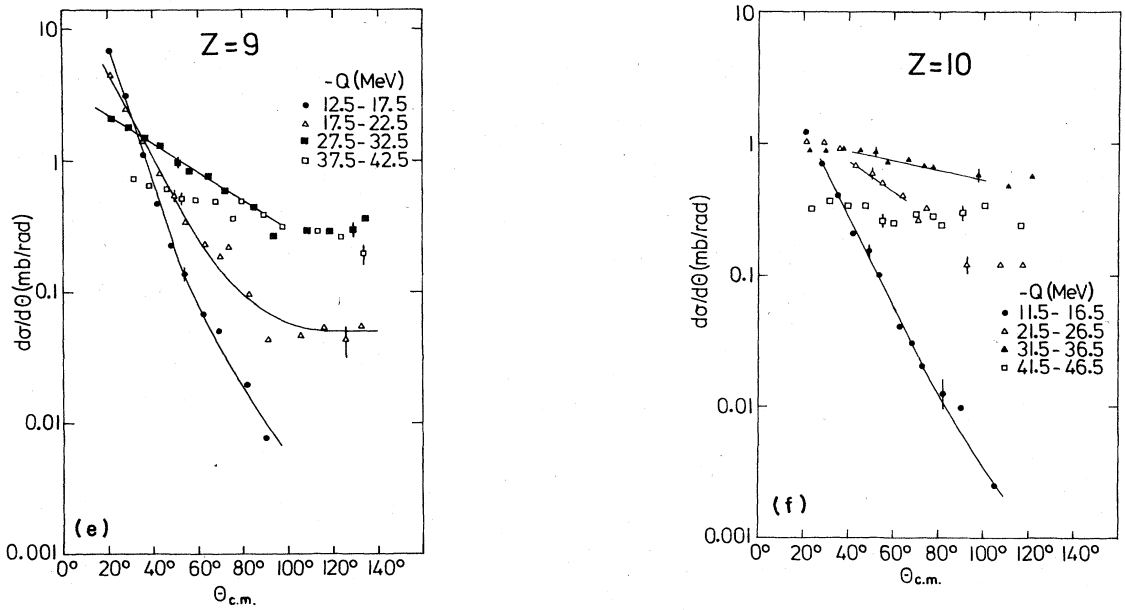

FIG. 4. (*Continued.*)

sections in the c.m. frame are integrals of $d^2\sigma/d\theta dE$ over the given Q windows of 5 MeV width. For the sake of transparency, a few Q windows have been omitted. As mentioned in Sec. II, contributions from sequential decay may become relevant in the $Z=9$ and 10 channels while the given numbers refer to an assumed two-body kinematics. The corresponding two-body $|Q|$ values for the unstable primary ejectile are generally smaller than the given values for the detected ejectile, e.g., by 8 MeV (5 MeV) for ^{20}Ne, originating from sequential α decay of ^{24}Mg, with an apparent two-body Q value of -45 MeV at $\theta_{c.m.}=40°$ (80°). In these examples, the primary c.m. scattering angles are dispersed over $\pm 12°$ by α emission at threshold, with mean values close to the ones given for ^{20}Ne.

A monotonic decrease with increasing angle is observed in all cases. The slope generally decreases with increasing inelasticity. But even in the most inelastic reactions $d\sigma/d\theta$ is found to be significantly different from being isotropic, i.e., the system is still far from the compound nuclear limit. No grazing peaks appear in the quasielastic transfer channels, unlike similar systems at lower bombarding energy.[27,28]

By comparison of the present system with $^{16}O+^{58}Ni$ (Ref. 29) and with $^{16}O+^{27}Al$ (Ref. 6) at $E_{c.m.}$ correspondingly to roughly three times the interaction barrier, it is found that the slope of the DI differential cross section decreases with decreasing atomic number of the target. This suggests that the tendency to rotate towards larger negative angles increases with decreasing charge product and/or with increasing angular velocity of the double nucleus. Deep-inelastic processes of the "orbiting"-type characterized by an isotropic $d\sigma/d\theta$ in the backward-angle region, as have been observed in ^{12}C- and ^{16}O-induced reactions on *sd*-shell nuclei,[14,30] fit into this systematics. Indeed, the DI differential cross sections in Fig. 4 become significantly flatter with $\theta_{c.m.}$ increasing beyond 100°. In several cases, $d\sigma/d\theta$ is consistent with being constant at the largest three or four scattering angles covered by this experiment.

The angle-integrated cross section in Table I has been obtained by extrapolation of $d\sigma/d\theta$ to 0°, using a Gaussian shape of the nonisotropic part. Guided by Fig. 2 and by the systematics of the most probable Q values, discussed in Sec. V, we have chosen with some arbitrariness an upper limit for the DI exit-channel energy which is 24 MeV above the interaction barrier for spheres. The total DI cross section of 230 mb is small in comparison with the calculated[10,11] cross section for fusion of 1300 mb. It accounts for about one-third of the difference between σ_{fusion} and the reaction cross section corresponding to $l_{graz}=50\hbar$. The orbiting component constitutes about one-third of the total DI cross section.

TABLE I. Angle-integrated deep-inelastic cross sections with $E_f \leq V_B+24$ MeV, using V_B of Eq. (9), and the contributions from "orbiting" to these cross sections.

Z	σ_{DI} (mb)	$\sigma_{orbiting}$ (mb)
5	21± 2	6±3
6	103±10	27±3
7	39± 4	10±3
8	50± 5	15±2
9	10± 1	4±1
10	8± 1	4±1

IV. SEMICLASSICAL PARAMETRIZATION OF THE ANGULAR DISTRIBUTIONS

Near-side–far-side decompositions of the differential cross section in heavy-ion reactions have been derived in the framework of direct-reaction theory, e.g., in Refs. 31–35. A rather simple form was obtained by Strutinsky[31] for the case of a peripheral reaction at large orbital angular momenta. In the helicity representation one may use a partial-wave expansion of the scattering amplitude which is of the same form as in the case of elastic scattering,

$$f(\theta)=\frac{1}{2ik}\sum_l (2l+1)S_l P_l(\cos\theta)\ , \tag{1}$$

provided that $|\underline{l}_i-\underline{J}_f| \ll l_i$ holds for the magnitudes of the total angular momenta in the entrance and exit channels, $\underline{l}_i$ and $\underline{J}_f=\underline{l}_f+\underline{I}_1+\underline{I}_2$ (see Ref. 32). This condition, which is proven true in the present case by the experimental spin alignment,[13,14] means that the reaction takes place essentially in a plane. Using three approximations, (i) the asymptotic form of the Legendre polynomials, (ii) replacement of the sum over l by an integral, and (iii) expansion of the phase δ_l of the partial-wave amplitudes $S_l=|S_l|\exp(i\delta_l)$ to second order about the mean partial-wave number l_0, Strutinsky obtains

$$\frac{d\sigma}{d\theta}=|f(\theta)|^2 \sim \exp\left[-\frac{(\theta_0-\theta)^2}{\xi^2}\right]+\exp\left[-\frac{(\theta_0+\theta)^2}{\xi^2}\right] + \text{interference term}\ , \tag{2}$$

where

$$\theta_l=\frac{d\delta_l}{dl}\ , \tag{3}$$

$$\theta_0=\theta_{l=l_0}\ , \tag{4}$$

$$\xi^2=\frac{2}{\Delta^2}+\frac{1}{2}\left[\frac{d\theta_0}{dl}\Delta\right]^2\ , \tag{5}$$

and Δ is the width in l space of the magnitudes of the partial-wave amplitudes in a Gaussian parametrization,

$$|S_l|=|S_{l_0}|\exp\left[-\frac{(l-l_0)^2}{\Delta^2}\right]\ . \tag{6}$$

Alternatives to this parametrization have also been discussed.[31,35] This form of $d\sigma/d\theta$ has an obvious interpretation[31] in terms of contributions from both sides of the interaction region, peaking at θ_0 and $-\theta_0$. The width of the fluctuations about these mean angles is given by Eq. (5). It has two contributions, the first one accounting for the quantum-mechanical uncertainty and the second one for the dynamical (classical) dispersion in the relevant l window. With increasing Δ, the first one decreases and the second one increases. While θ_l defines the deflection function at the fixed reaction Q value, the mean angle θ_0 represents, as a function of Q, the deflection function of the frictional process.

If the sum over l in Eq. (1) is evaluated by means of the exact Poisson summation technique, instead of replacing it by an integral, the first two terms on the right-hand side (rhs) of Eq. (2) are retained and additional terms are found, arising from waves that have encircled the nuclear surface once or several times.[36,37] We associate these with the orbiting contributions discussed in the preceding section.

Full coherence of the partial waves was employed in the preceding, as is adequate for direct reactions. Multistep direct-reaction theory has recently been applied to DI reactions, in particular to the reaction investigated here, with emphasis on the transition from QE to DI reactions.[38,39] A near-side–far-side decomposition was shown to be feasible in this theoretical framework.[39] A good description of the data was obtained for (^{16}O,^{16}O′) at $Q \gtrsim -20$ MeV.

In DI reactions, the measured $d\sigma/d\theta=\langle |f(\theta)|^2\rangle$ is a twofold average over many unbound states, covered by the chosen Q window, and over the energy dispersion of the incoming beam. Such an averaging over rapidly changing phases results in a partial loss of the coherence in the transition probabilities $\langle |S_l S_{l'}^*| \rangle$, as discussed in Refs. 40–42. In this respect, the DI reactions are intermediate between the extreme cases of a direct reaction and of a compound nuclear reaction where the different partial waves are incoherent, $\langle |S_l S_{l'}^*| \rangle=\delta_{l,l'}$. With these considerations, the form of Eq. (2) could be recovered[41,42] with a modified form for the dynamical-dispersion term in Eq. (5).

In the treatment of DI reactions, the interference of the near-side and far-side contributions in Eq. (2) is usually assumed to be negligible[40–42] because of their opposite mean polarizations along the scattering normal and because of the averaging already discussed. This is in agreement with the absence of diffraction structure in the experimental angular distributions (Fig. 4).

We have used the resulting form of the angular distribution,

$$\frac{d\sigma}{d\theta}=c\left\{\exp\left[-\frac{(\theta_0-\theta)^2}{\xi^2}\right]+\exp\left[-\frac{(\theta_0+\theta)^2}{\xi^2}\right]\right\} + \left[\frac{d\sigma}{d\theta}\right]_{\text{orbiting}}\ , \tag{7a}$$

$$=c'\exp(-\theta^2/\xi^2)\cosh(2\theta\theta_0/\xi^2) + \left[\frac{d\sigma}{d\theta}\right]_{\text{orbiting}}\ , \tag{7b}$$

to parametrize our data. The angle-independent contribution from orbiting was determined as the average of $d\sigma/d\theta$ at those backward angles where it is consistent with being constant. The angle-integrated cross sections which determine the constant in Eq. (7) are listed in Table I.

The shape of the forward-peaking term in Eq. (7b) is fixed by two parameters, ξ^2 and θ_0, but it is not equally sensitive to these. For $|\theta_0| \lesssim \xi/\sqrt{2}$, the slope is essentially determined by the spreading width ξ^2. The second

parameter is affected rather strongly by small deviations from the Gaussian form of the near- and far-side contributions. Only if a peak were observed at $\theta \neq 0°$ could one reliably extract the mean deflection angle θ_0 from the angular distributions alone. However, by including the independent information from the γ-ray circular polarization experiment,[15] both the deflection angle and the spreading width can be determined. Since the mean total spin transfers are oppositely oriented in the near- and far-side components, the polarization (along $\underline{k}_i \times \underline{k}_f$) is a measure of the relative intensities of these components. If $-|P_\gamma(\theta)|^{\max}$ and $+|P_\gamma(\theta)|^{\max}$ designate the circular polarization of the near- and the far-side components, respectively, defined by the maximum polarization allowed by the spin alignment,[14,15] the measured $P_\gamma(\theta)$ may be expressed as

$$P_\gamma(\theta)/|P_\gamma(\theta)|^{\max} = -\tanh(2\theta\theta_0/\xi^2) \times \left[1 - \left[\frac{d\sigma}{d\theta}\right]_{\text{orbiting}} \Big/ \frac{d\sigma}{d\theta}\right]. \quad (8)$$

The first factor is the difference of the far-side and the near-side contributions in Eq. (2) divided by their sum. It accounts for the loss of polarization by the angular spreading across the beam direction.[43] The second factor results from the vanishing polarization of the orbiting component, which is of particular importance for the most inelastic processes at large angles as discussed in Ref. 15. We have determined θ_0/ξ^2 and ξ^2 by fitting Eq. (8) to the measured circular polarization and Eq. (7b) to the measured differential cross section, respectively.

The resulting parameters are listed in Table II, which is confined to the two strongest reaction channels, due to the statistics of the polarization experiment, and to $Q < -20$ MeV, since $|P_\gamma|^{\max}$ is not well defined experimentally for less inelastic processes. Only the range of $\theta_{\text{lab}} < 50°$ was taken into account by the fit because significant, though small, deviations from the double-Gaussian form were found at larger angles. Good fits of the angular distributions and of the polarizations were obtained in all cases. As an example, Fig. 5 shows the DI differential cross sections in the $Z=6$ channel and the fit curves with their decomposition according to Eq. (7a). Because of the dispersion about 0°, considerable near-side contributions to the dominant far-side component are present at forward angles. The contributions from orbiting are larger than those from near-side scattering beyond 40° for -30 MeV $> Q > -40$ MeV and beyond 15° for -40 MeV $> Q > -50$ MeV.

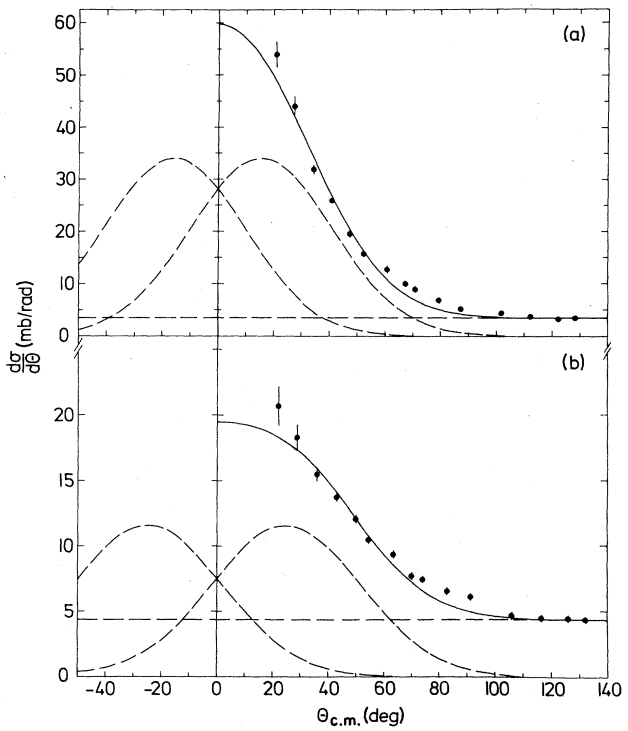

FIG. 5. Differential cross section in the center-of-mass frame for carbon ejectiles with -40 MeV $\leq Q \leq -30$ MeV (a) and -50 MeV $\leq Q \leq -40$ MeV (b), semiclassical fit curve (full line) with parameters given in Table II, and its decomposition (dashed lines) according to Eq. (7a) into the near-side, the (dominant) far-side, and the orbiting component.

TABLE II. Semiclassical parameters derived from a fit of the angular distributions and the polarizations with Eqs. (7) and (8), respectively.

Z	$-Q$ (MeV)	ξ[a] (deg)	θ_0[b] (deg)
6	20–30	30.0±1.0	− 5±2
	30–40	35.2±1.1	−16±8
	40–50	38.2±0.8	−25±8
8	20–30	24.9±0.9	− 9±9
	30–40	37.0±1.2	−17±6
	40–50	>35	

[a]Half-width at $1/e$ of the maximum in each component, the near-side and the far-side one.
[b]Mean deflection angle.

The results obtained for the $Z=6$ and 8 channels are the same within the uncertainty of our procedure (Table II). As expected for a frictional process leading to negative angles, the mean negative deflection angle increases with increasing inelasticity. However, the spreading width increases as well so that ξ is larger than θ_0 in all cases. Since the fluctuations are larger than the mean deflection, an interpretation of the angular distributions in terms of only the deflection function would be insufficient. To find out the origin of such a large angular dispersion, one may solve Eq. (5) for Δ^2 by using a calculated deflection function. As holds generally for the two solutions of this quadratic equation, the smaller value Δ^2 corresponds to a dominance of quantal dispersion and the larger one to a dominance of the classical dispersion, expressed by the first and the second term, respectively, on the rhs of Eq. (5). Such an ambiguity has already been discussed in the case of quasielastic reactions.[44,45] Using a deflection function[15] based on an energy-density nuclear potential and strong-friction parameters, which accounts for the total yield from negative-angle scattering,[15] we find that the two solutions are quite close to each other in

the present case. The resulting half-width at $1/e$ of the maximum of the l distribution, Eq. (6), is $\Delta=3\hbar$. This means that the quantal and classical spreading are equally important in the present case. This result is expected to hold quite generally for the flat deflection functions demanded by $l_{\text{graz}}=50\hbar$ and $l_{\text{crit}}=41\hbar$ and the total yield of negative-angle scattering. In the case of much heavier systems we expect the classical dispersion term to dominate since the larger cross section for DI reactions[1,2] requires a larger range of contributing partial waves. A semiclassical analysis of 380-MeV Ar + Th confirms this expectation.[43] In light systems, however, the angular distributions in DI reactions result from the joint classical and quantal dispersion.

V. ENERGY DISSIPATION AND FRAGMENT DEFORMATION

In the angular range of $\theta_{\text{lab}}=60°-110°$, the most probable Q values and the shapes of the energy spectra in the DI region are found to be consistent with being independent of the angle. This indicates that complete relaxation of the energy is reached in each reaction channel with atomic number Z of the detected ejectile. The extracted most probable values E_f^0 of the exit channel energy, $E_f^{\text{c.m.}}=E_i^{\text{c.m.}}+Q$, are plotted in Fig. 6 as a function of Z. The mean values of $E_f^{\text{c.m.}}$ agree with the most probable ones within ±1 MeV in the considered range of $\theta_{\text{lab}}=60°-110°$, where the shapes of the spectra are not far from being symmetric. However, because of the corrections at low $E_f^{\text{c.m.}}$ due to light-element contaminations of the target and because of the presence of a very weak QE component even at large angles (see Sec. VI), we consider the mean values of the DI exit-channel energies as not so well defined experimentally as the most probable ones.

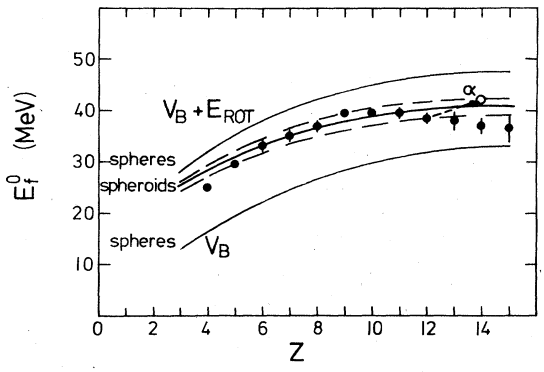

FIG. 6. Most probable deep-inelastic exit-channel energy as a function of the atomic number of the detected fragment. The dashed arrow shows the estimated effect of α evaporation on the primary most probable energy, which is only significant for $Z>9$. The calculated curves represent the interaction barrier for spheres and the sum of the barrier and of the relative-motion rotational energy in the cases of rigidly rotating spheres and spheroids with an axis ratio $a/b=1.4$ (full line), 1.3, and 1.5 (upper and lower dashed line, respectively). In the case of spheres the barrier has been approximated by V_B defined in Eq. (9).

The considerable distance between the data points and the interaction barrier for spheres, approximated (see the following) in Fig. 6 by

$$V_B=\frac{Z_1Z_2e^2}{[1.225(A_1^{1/3}+A_2^{1/3})+2]\text{ fm}}\ , \tag{9}$$

gives clear evidence of the rotational energy remaining in the relaxed system. On the other hand, the sum of V_B and of the rotational energy of relative motion of spheres performing rigid rotation at a total angular momentum of $42\hbar$ clearly overestimates E_f^0. This indicates that the fragments are deformed at the scission point. The most probable entrance-channel angular momentum is chosen to be $l_{\text{crit}}+1\hbar$ with the sharp cutoff value $l_{\text{crit}}=41\hbar$ taken from a model that describes fusion cross sections in several similar systems.[10,11] The choice of l_i only one unit above l_{crit} is motivated by the small total DI cross section (Table I). For a detailed analysis we decompose the most probable exit-channel energy according to

$$E_f^0=l_f(l_f+1)/2\mu D^2+V(D)\ . \tag{10}$$

In this way we define for a given exit channel a separation D outside of which the relative motion is subject to the conservative forces only. Equation (10) implies that the radial velocity is negligible at this point.

We use a double-folding potential $V(r)$ with parameters fitted to many data, including fusion cross sections and elastic-scattering differential cross sections.[46] This potential depends in a transparent manner on the deformation via the curvature at the touching point. We parametrize the deformation in terms of the axis ratio a/b of ellipsoids with fixed volume given by the sharp-surface spheres with radii[46] $R_i=1.16A_i^{1/3}$ fm. The axis of symmetry is directed along the line connecting the centers of mass. The Coulomb part of the potential depends on the deformation by the following approximation to the exact result[47] of double folding:

$$V_{\text{Coul}}(r)\approx\frac{Z_1Z_2e^2}{r}\left[1+\frac{6}{5}\frac{a-b}{a+2b}\frac{R_1^2+R_2^2}{r^2}\right]\ . \tag{11}$$

The total potential $V(r)$ has a maximum at a separation of about a_1+a_2+2 fm. The nuclear part is rather small at this maximum with a magnitude less than 2 MeV. For spheres the height of the maximum is reproduced approximately by the "Coulomb barrier" given in Eq. (9).

In the spirit of strong friction models,[48,49] we assume that the radial and the orbital motion are completely damped until the separating system reaches the barrier of $V(r)$ and that only conservative forces are relevant outside the barrier, i.e., we identify D in Eq. (10) with the separation at the barrier and calculate l_f from the condition of sticking at this separation,

$$l_f=\frac{\mu D^2}{\mu D^2+\Theta_1+\Theta_2}l_i\ . \tag{12}$$

The intrinsic moments of inertia are obtained[50] in the same framework as the nuclear potential as

$$\Theta_i = 0.2 A_i R_i^2 \left[\left[\frac{a}{b} \right]^{4/3} + \left[\frac{b}{a} \right]^{2/3} \right] + 2A_i \ , \quad (13)$$

in units of u fm^2. The deformation a/b, which is the only free parameter in this simple approach, is now adjusted via Eq. (10) to the measured E_f^0.

In the strong-friction models the frictional force reaches as far out as the nuclear force, i.e., slightly further out than the separation at the barrier. However, because of the smooth curvature of $V(r)$ and because of the small radial velocity, this will not seriously affect our results as far as the radial motion is concerned. With respect to the tangential friction, an important check of our procedure is provided by the observed angular-momentum transfer.[13,14] The experimentally determined heavy-fragment spins are reproduced well by inserting the separation D ($\approx a_1 + a_2 + 2$ fm) derived from E_f^0 into Eq. (12). This agreement is even improved if the nonaligned spin is taken into account which increases the heavy-fragment spin, e.g., in the $Z=6$ channel, by $2\hbar$ with respect to the sticking spin of $14\hbar$. In contrast to the strong-friction picture, a much smaller complete-damping radius, close to the critical radius for fusion, has been proposed as a possible alternative.[51] It has been pointed out[51] that fits of the experimental exit-channel energies, carried out[7,52] in a similar fashion as here, become ambiguous if the assumption of strong friction is abandoned. However, with the alternative small complete-damping radius, the angular momentum transfer is strongly overestimated in our case. Furthermore, the amount of negative-angle scattering could not be reproduced in trajectory calculations unless a strong friction at rather large radius was used.[15] We conclude that with two observables, E_f^0 and the angular-momentum transfer, the scission configuration is rather well determined if we accept that the ellipsoidal parametrization is valid at $r=D$ (which of course does not exclude neck formation at smaller separation). Regarding the sensitivity of our procedure to the choice of l_i, we note that the calculated rotational energy at $r=D$ of 12 to 14 MeV for $Z=15$ to 4, respectively, will change by 10% if $l_i = 42\hbar$ is changed by $2\hbar$.

The best fit of the experimental values of E_f^0 was obtained with an axis ratio $a/b=1.4$, corresponding to a deformation parameter

$$\beta = \left[\frac{4\pi}{5} \right]^{1/2} \frac{1-b/a}{0.5+b/a} = 0.37 \ .$$

The fit curve is shown in Fig. 6 together with those curves obtained by increasing (lower dashed curve) and decreasing (upper dashed curve) the extracted value of a/b by 0.1, which indicates the uncertainty of our procedure. In the strong $Z=5$–8 DI channels, E_f^0 is described well by the band defined by the dashed curves. The same deformation was used for the light and for the heavy fragment despite the differences in nuclear structure. The smooth Z dependence of the experimental points indicates that the dynamical deformation at the scission point is not very sensitive to the different ground-state deformations of the light ejectiles. Use of a spherical shape for the light fragment would increase the axis ratio a/b of the heavy fragment by 0.1. The apparent decrease of E_f^0 with increasing $Z \geq 12$ is attributed to the effect of particle evaporation which may be approximated by

$$E_{\text{lab}}(Z_{\text{primary}}) = E_{\text{lab}}(Z) M_{\text{primary}} / M \ .$$

This is exemplified in Fig. 6 by the case of one-α evaporation from a primary $Z=14$ fragment. We find all E_f^0 values from $Z=5$ up to $Z=15$ (symmetric splitting) consistent with $a/b = 1.4 \pm 0.1$. However, a tendency of E_f^0 to decrease more steeply with decreasing Z is observed for $4 \leq Z \leq 8$, indicating a slight increase of the deformation with increasing mass of the targetlike fragment.

VI. SURPRISAL ANALYSIS OF THE ENERGY SPECTRA

In an information-theoretic approach, continuum spectra of heavy-ion reactions have been described as maximum-entropy distributions subject to constraints.[18,19] Given the phase space of all final quantum states allowed by the conservation laws, the complete information on the reaction dynamics contained in the experimental spectra is expressed by these, generally very few, constraints. The procedure of a constrained phase-space analysis, discussed extensively in Ref. 19, is briefly summarized here and then applied to the observed energy spectra.

A measure of the deviation of an observed energy spectrum at a given angle, $d\sigma/d\Omega(E_f)$, from a purely statistical distribution, $d\sigma^0/d\Omega(E_f)$, i.e., of the deviation from a uniform population of the accessible phase space, is provided by the surprisal which is defined as

$$\text{surprisal}(E_f) = -\ln \left[\frac{d\sigma}{d\Omega}(E_f) \Big/ \frac{d\sigma^0}{d\Omega}(E_f) \right] . \quad (14)$$

In a two-body reaction the purely statistical spectrum $(d\sigma^0/d\Omega)(E_f)$ is given by the product of the convoluted level densities of both fragments and of the density of translational states. Since the latter is proportional to $\sqrt{E_f}$ and since the light fragment's share of the total excitation energy is very small and only weakly dependent on E_f,[13,14] the shape of $(d\sigma^0/d\Omega)(E_f)$ is essentially given by the level density, $\rho(E_x)$, of the heavy fragment which rapidly increases with the excitation energy, $E_x \approx E_i - E_f + Q_{gg}$. Therefore, the surprisal is given in good approximation by the logarithm of the ratio of the measured particle yield and the heavy fragment's level density

$$\text{surprisal}(E_x) = -\ln[N(E_x)/\rho(E_x)] + c \ , \quad (15)$$

with normalization constant c which is not of interest here.

If the experimental distribution is not purely statistical, as becomes obvious by a nonconstant surprisal, constraints are present. Constraints are given in terms of mean values $\langle A_i(E_x) \rangle$ of certain functions $A_i(E_x)$ of the variable E_x. For these functions, which are not specified by information theory, one has to make an ansatz which

may be guided by models of the reaction dynamics. For instance, a constraint on the energy itself is suggested by the classical orbit-matching condition. If the set of constraints is complete, the spectrum is reproduced by

$$N(E_x)=c'\rho(E_x)\exp\left[-\sum_i \lambda_i A_i(E_x)\right], \tag{16}$$

with Lagrange multipliers λ_i determined by the requirement

$$\text{surprisal}\,(E_x)=\lambda_0+\sum_i \lambda_i A_i(E_x), \tag{17}$$

for all E_x.

In practice, with an incomplete set of constraints, the distribution of maximum entropy is still given by Eq. (16) but with parameters λ_i that minimize the amount of

$$\int_{E_x}\left[\lambda_0+\sum_i \lambda_i A_i(E_x)-\text{surprisal}\,(E_x)\right]N(E_x)dE_x\ . \tag{18}$$

This means that a fit of the surprisal by means of the rhs of Eq. (17) is performed such that the total of the deviations weighted by $N(E_x)$ is minimal. In this way, the experimental spectra are conceived as maximum-entropy distributions with mean values $\langle A_i(E_x)\rangle$. These are given by the fit parameters λ_i according to

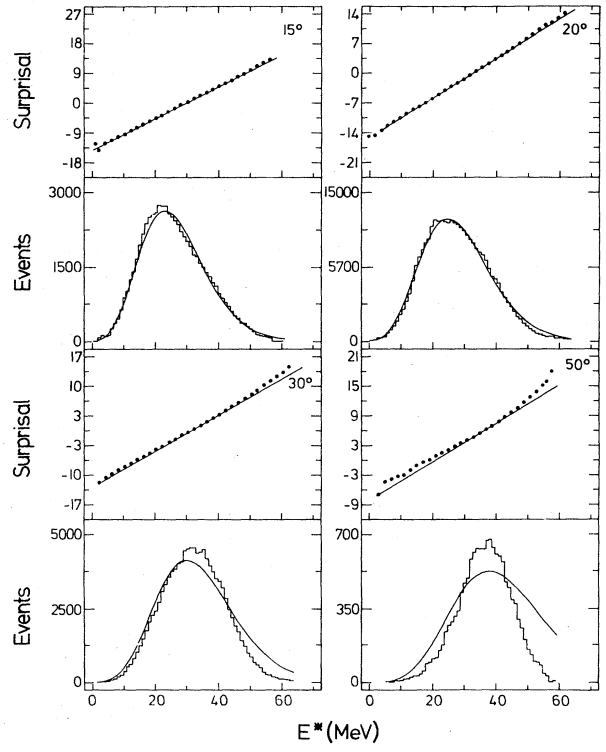

FIG. 7. Energy spectra of carbon ejectiles at different scattering angles in the laboratory frame (lower panel histograms) and the corresponding surprisals (upper panel points) extracted by means of Eq. (15) using a level density with fixed rotational energy. The full lines represent the results of the weighted linear fits to the surprisal which yield the mean excitation energy of the heavy fragment as the only constraint. ($E^*=-Q-1.6$ MeV in the present case.)

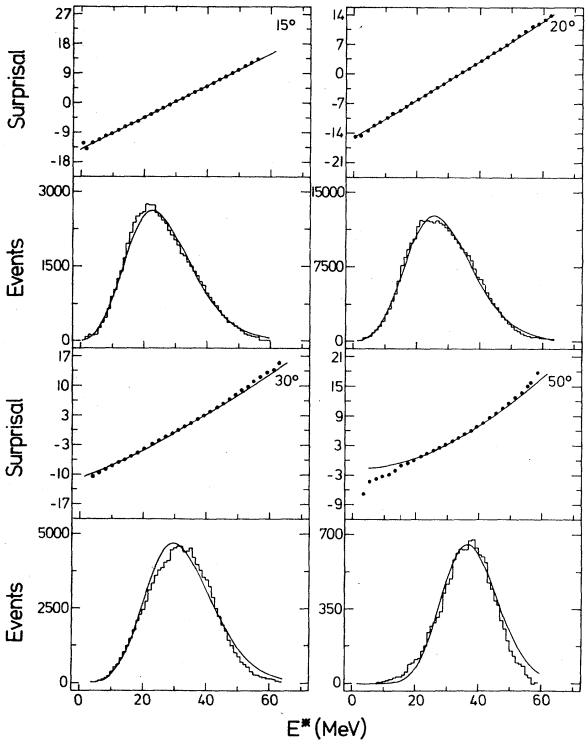

FIG. 8. Energy spectra and surprisals as in Fig. 7 with full lines representing the results of quadratic-form fits to the surprisals. The additional constraint, as compared to Fig. 7, is given by the mean value of $\sqrt{E^*}$.

$$\langle A_i(E_x)\rangle=\frac{\int_{E_x} A_i(E_x)\rho(E_x)\exp\left[-\sum_i \lambda_i A_i(E_x)\right]dE_x}{\int_{E_x}\rho(E_x)\exp\left[-\sum_i \lambda_i A_i(E_x)\right]dE_x}\ . \tag{19}$$

We have applied this formalism to the $Z=6$ energy spectra at various angles. In Figs. 7–9 these spectra are shown in the lower panels and the surprisals, derived according to Eq. (15), in the upper panels. In all cases, we have used a Fermi-gas type of level density,[53]

$$\rho(E^*,J)\sim(E^*)^{-5/4}\exp(2\sqrt{aE^*})(2J+1)\times\exp[-(J+\tfrac{1}{2})^2/2\sigma^2]\ , \tag{20}$$

with $E^*=E_x-E_{\text{pairing}}$. In the case of the ^{48}Ti(^{16}O,^{12}C)^{52}Cr reaction, $E_{\text{pairing}}=3.8$ MeV and $Q_{gg}=2.2$ MeV so that $E^*=-Q-1.6$ MeV. We shall first (Figs. 7 and 8) use a constant $J=J_{\text{sticking}}$ so that the effect of the rotational energy on the level density is taken into account only approximately.[18,19] We shall then (Fig. 9) demonstrate how the results of the surprisal analysis change if the knowledge[13,14] of the correlation between E^* and J is taken into account.

A roughly linear increase of the surprisal with increasing E^* is observed (Fig. 7). This indicates that the dominant constraint is on the mean value of E^*, as in the

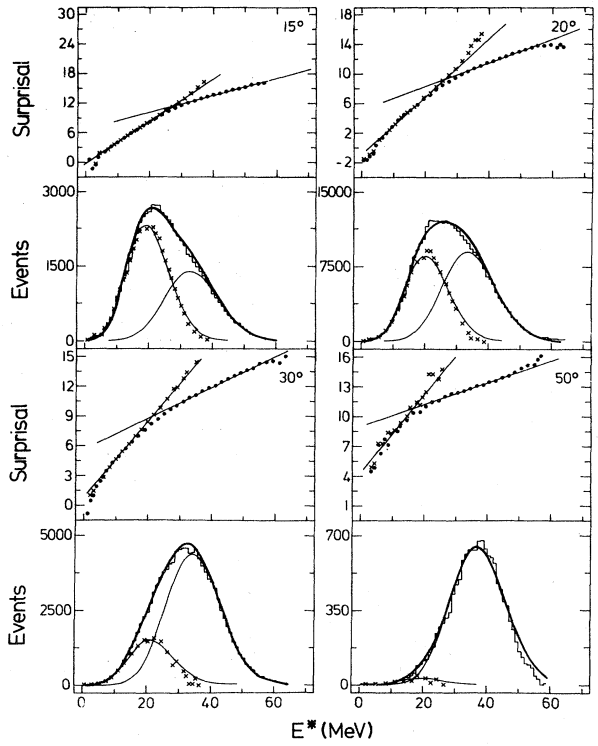

FIG. 9. Energy spectra as in Fig. 7 and surprisals extracted by means of Eq. (15) using a level density that takes the Q dependence of the spin transfer into account. The light lines represent one-constraint fits to the two reaction components. The differences between the experimental spectra and those derived from the linear surprisals of the deep-inelastic component, as well as the surprisals corresponding to these differences, are given by $\times$ symbols. The heavy lines in the lower panels represent the results of the combined fit of both components.

cases studied in Refs. 18 and 19. A linear fit, minimizing the integral over

$$[\lambda_0+\lambda_1 E^* - \text{surprisal}(E^*)]N(E^*)$$

as a special case of expression (18), accounts well for the energy spectra and their surprisals at forward angles $\theta_{\text{lab}} < 30°$. The gradual decrease of the slope of the surprisal with increasing angle reflects the increase of $\langle E^* \rangle$, according to the increasing weight of the DI reaction component. It is noted, however, that no two-component characteristics become apparent in these surprisals. At larger angles, $\theta_{\text{lab}} \geq 30°$, where the DI component predominates, the width is overestimated by the linear fit. Furthermore, the experimental spectra are less asymmetric at these angles than the ones derived from the linear surprisal fit.

The curvature of the surprisals at $\theta_{\text{lab}} \geq 30°$ indicates the presence of another constraint. Following Ref. 19 we have imposed the second constraint on $\langle \sqrt{E^*} \rangle$. In this way, three free Lagrange parameters, λ_0, λ_1, and λ_2, are fitted at each angle. A satisfactory fit of the surprisals and of the corresponding energy spectra is obtained at all angles (Fig. 8). The results at $\theta_{\text{lab}}=30°$ resemble closely those obtained[19] for the $Z=6$ channel from 96-MeV $^{16}O+Ni$ at 40°. In both cases the surprisal is weakly upward bent.

The second constraint was shown[19] to arise from a constrained width of the distribution of exciton numbers of the excited nucleus (as opposed to a constrained mean exciton number which is equivalent to the constraint on E^*, the first constraint). However, it is not easy to see why such a constraint should be of importance in the DI reaction component. The mean value of the energy loss and of the angular momentum loss are relaxed over a large angular range. Moreover, the spin axis fluctuations about the mean spin vector are consistent with an equilibrated distribution.[13,14]

It is, however, possible to avoid the second constraint in the present case if the knowledge on the correlation between energy and angular-momentum loss is taken into account. The angular momentum transfer, deduced from particle-γ coincidence studies,[13,14] increases with the energy loss in the DI region by about $1\hbar$ per 4 MeV. We have inserted this linear relation of J and E^* into the level density, $\rho(E^*,J(E^*))$, in Eq. (20). The resulting surprisals (Fig. 9) differ from the ones already discussed and are suggestive of a two-component analysis. A linear fit with one constraint on the most probable Q value in the QE region and another one in the DI region accounts well for these surprisals and for the energy spectra. At 15° and 20°, which are close to $\theta_{\text{graz}}=19°$, both components are of similar strength. With increasing angle, the quasielastic component decreases rapidly in intensity. Yet, its presence becomes clearly apparent in the surprisal at 30° and even at 50°. At these angles the energy distributions are even better reproduced than with the two-constraints fit of Fig. 8.

The excitation energies at which both components are equally strong are not far from the borderline between positive- and negative-angle scattering (dashed line in Fig. 2). They reproduce the ascent of this borderline with increasing angle. However, because of the angular dispersion about 0° in both components, their relative weights are not related in a simple manner to the relative contributions from positive- and negative-angle scattering. The mean $|Q|$ value of the DI component (Table III) increases weakly with increasing angle. Already at 15°, it is not far (6 MeV) below the relaxation value (Sec. V) reached at large angles, which indicates that the frictional energy loss occurs rather rapidly in between $\pm\theta_{\text{grazing}}$.

TABLE III. Results of the one-constraint fits to the surprisals of the two reaction components, obtained with a level density incorporating the Q-dependent spin transfer.

	Quasielastic		Deep inelastic	
θ_{lab}	λ_1	$\langle E^* \rangle^a$	λ_1	$\langle E^* \rangle^a$
15°	0.421	20.2	0.176	33.9
20°	0.414	20.5	0.180	33.6
30°	0.380	22.0	0.160	35.0
50°	0.429	19.8	0.130	37.2

[a] $E^* = E_x - E_{\text{pairing}} = -Q - 1.6$ MeV.

The weak increase with increasing θ may be due to a slow relaxation in the shape degrees of freedom. The value of $\langle E^* \rangle$ at 30° is close to what is expected for complete damping in the case of no deformation (given by $V_B + E_{\text{rot}}$ in Fig. 6). For angles larger than 60° the fitted $\langle E^* \rangle$ is consistent with the most probable Q value for complete damping, discussed in Sec. V. In the quasielastic component, the extracted constraint is in good agreement with the expectation for a matched one-step α transfer, $Q_{\text{opt}} = -23$ MeV.

The approach followed in Fig. 9, in comparison with the one described earlier, is not to be considered as controversial in terms of information theory. However, it demonstrates the benefit of taking as much experimental information as possible into account in such an analysis. Unless a total multidimensional surprisal analysis of all observables can be made, it appears reasonable to use a phase space subjected to the known correlations of the variable under investigation with other variables. In view of the richness of phenomena in the distributions of the reaction products with respect to the angle, mass, charge, angular momentum, and m-substate quantum number, a surprisal analysis of the energy spectra alone is not expected to furnish a complete understanding of the reaction mechanism. However, the value of this technique in the present example becomes apparent by the following results:

(1) The two-component characteristics can be traced over a large angular range in a case where such a decomposition is not apparent in the measured spectra.

(2) The DI energy distribution is in accordance with the distribution of maximum entropy about the mean energy loss.

VII. SUMMARY

Doubly differential cross sections were measured for reactions induced by 100-MeV ^{16}O on ^{48}Ti. These were analyzed in terms of mean energy losses and deflection angles and of fluctuations about the mean values of both. Three different approaches were used: a semiclassical analysis of the angular distributions, a macroscopic analysis of the energy losses, and a statistical analysis of the energy spectra. The interplay of these aspects is essential to produce the observed cross section distributions.

The evolution of the reaction process from quasielastic scattering to complete damping was found to be associated with a continuous broadening of the angular distributions. These were decomposed into near-side, far-side, and isotropic (orbiting) contributions. In the DI reaction component the magnitude of the mean deflection angle in the dominant far-side component increases with increasing inelasticity, in agreement with macroscopic models developed for heavier systems.[49] However, the angular width of the dispersion about the mean trajectory was found to be larger than the mean angle in our semiclassical analysis. Quantal and dynamical fluctuations were argued to be of comparable magnitude in the present system.

The most probable energy losses at large angles were interpreted in terms of complete damping of the relative motion at the barrier of the potential $V(r)$ in the different exit channels. From the energy balance, including the rotational energy of relative motion in the sticking configuration, we deduced a considerable deformation at scission.

A constrained-phase-space approach led to a division of the $Z=6$ energy spectra into the QE direct reaction component and the many-step DI component with mean Q values in accordance with the classical conditions for orbit matching and for complete relaxation, respectively. The shapes of the spectra were found to be consistent with distributions of maximum entropy about the mean Q values of either component.

ACKNOWLEDGMENTS

Helpful discussions with Dr. K. Hartmann are gratefully acknowledged. This work was supported by the Bundesministerium für Forschung und Technologie.

*Present address: Brookhaven National Laboratory, Upton, NY 11973.

[1]V. V. Volkov, *Lecture Notes in Physics,* Vol. 33 (Springer, Berlin, 1975), p. 254; Phys. Rep. **44**, 93 (1978).

[2]W. U. Schröder and J. R. Huizenga, Annu. Rev. Nucl. Sci. **27**, 465 (1977).

[3]R. Kaufmann and R. Wolfgang, Phys. Rev. **121**, 192 (1961).

[4]G. F. Gridnev, V. V. Volkov, and J. Wilczynski, Nucl. Phys. **A142**, 385 (1970).

[5]R. Albrecht, W. Dünnweber, G. Graw, H. Ho, S. G. Steadman, and J. P. Wurm, Phys. Rev. Lett. **34**, 1400 (1975).

[6]T. M. Cormier, A. J. Lazzarini, M. A. Neuhausen, A. Sperduto, K. Van Bibber, F. Videbaek, G. Young, E. B. Blum, L. Herreid, and W. Thoms, Phys. Rev. C **13**, 682 (1976).

[7]J. B. Natowitz, M. N. Namboodiri, R. Eggers, P. Gonthier, K. Geoffroy, R. Hanus, C. Towsley, and K. Das, Nucl. Phys. **A277**, 477 (1977).

[8]Nguyen Van Sen, J. C. Gondrand, F. Merchez, and R. Darves-Blanc, Phys. Rev. C **22**, 2424 (1980).

[9]Y. Nagame, H. Nakahara, K. Sueki, H. Kudo, I. Kohno, and M. Yanokura, Z. Phys. A **317**, 31 (1984).

[10]R. Bass, Nucl. Phys. **A231**, 45 (1974).

[11]M. N. Namboodiri, E. T. Chulik, J. B. Natowitz, and R. A. Kenefick, Phys. Rev. C **11**, 401 (1975).

[12]C. Lauterbach, W. Dünnweber, G. Graw, W. Hering, H. Puchta, and W. Trautmann, Phys. Rev. Lett. **41**, 1774 (1978).

[13]H. Puchta, W. Dünnweber, W. Hering, C. Lauterbach, and W. Trautmann, Phys. Rev. Lett. **43**, 623 (1979).

[14]W. Dünnweber, in *Nuclear Structure and Heavy Ion Dynamics,* Proceedings of the International School of Physics, "Enrico Fermi," edited by L. Moretto and R. A. Ricci (North-Holland, Amsterdam, 1984), p. 389.

[15]W. Trautmann, W. Dünnweber, W. Hering, C. Lauterbach, H. Puchta, R. Ritzka, and W. Trombik, Nucl. Phys. **A422**, 418

(1984).
[16]G. R. Young, K. A. Van Bibber, A. J. Lazzarini, S. G. Steadman, and F. Videbaek, Phys. Rev. C **25**, 1304 (1982).
[17]H. Ho, R. Albrecht, H. Damjantschitsch, F. J. Demond, W. Kühn, J. Slemmer, J. P. Wurm, D. Disdier, V. Rauch, F. Scheibling, and T. Døssing, Z. Phys. A **300**, 205 (1981).
[18]R. D. Levine, S. G. Steadman, J. S. Karp, and Y. Alhassid, Phys. Rev. Lett. **41**, 1537 (1978).
[19]Y. Alhassid, R. D. Levine, J. S. Karp, and S. G. Steadman, Phys. Rev. C **20**, 1789 (1979).
[20]L. C. Northcliffe and F. R. Shilling, Nucl. Data Tables **7**, 233 (1970).
[21]B. D. Wilkins, M. J. Fluss, S. B. Kaufman, C. E. Gross, and E. P. Steinberg, Nucl. Instrum. Methods **92**, 381 (1971).
[22]H. Ho, P. L. Gonthier, G. Y. Fan, W. Kühn, A. Pfoh, L. Schad, R. Wolski, J. P. Wurm, J. C. Adloff, D. Disdier, A. Kamili, V. Rauch, G. Rudolf, F. Scheibling, and A. Strazzeri, Phys. Rev. C **27**, 584 (1983).
[23]T. M. Cormier, Proceedings of the Symposium on Macroscopic Features of Heavy-Ion Collisions, Argonne, 1976, edited by D. G. Kovar, p. 153.
[24]J. Wilczynski, Phys. Lett. **47B**, 484 (1973).
[25]D. M. Brink, Phys. Lett. **40B**, 37 (1972).
[26]R. L. McGrath, T. M. Cormier, D. F. Geesaman, J. W. Harris, L. L. Lee, and J. P. Wurm, Proceedings of the Symposium on Macroscopic Features of Heavy-Ion Collisions, Argonne, 1976, edited by D. G. Kovar, p. 681.
[27]P. R. Christensen, V. I. Manko, F. D. Becchetti, and R. J. Nickles, Nucl. Phys. **A207**, 33 (1973).
[28]J. Wilczynski, K. Siwek-Wilczynska, J. S. Larsen, J. C. Acquadro, and P. R. Christensen, Nucl. Phys. **A207**, 147 (1974).
[29]P. D. Bond, C. Chasman, and A. Z. Schwarzschild, Proceedings of the Symposium on Macroscopic Features of Heavy-Ion Collisions, Argonne, 1976, edited by D. G. Kovar, p. 475.
[30]D. Shapira, J. L. C. Ford, J. Gomez del Campo, and P. H. Stelson, Phys. Rev. C **21**, 1824 (1980).
[31]V. M. Strutinsky, Phys. Lett. **44B**, 245 (1973); Zh. Eskp. Teor. Fiz. **46**, 2078 (1964) [Sov. Phys.—JETP **19**, 1401 (1964)].
[32]V. M. Strutinsky and S. M. Vydrug-Vlasenko, Z. Phys. A **294**, 281 (1980).
[33]W. E. Frahn, Nucl. Phys. **A272**, 413 (1976).
[34]W. A. Friedman, K. W. McVoy, and G. W. T. Shuy, Phys. Rev. Lett. **33**, 308 (1974).
[35]D. R. Dean and N. Rowley, J. Phys. G **10**, 493 (1984).
[36]N. Rowley and C. Marty, Nucl. Phys. **A266**, 494 (1976).
[37]K. Hartmann, W. Dünnweber, and W. E. Frahn, Nucl. Phys. **A380**, 170 (1982).
[38]H. Lenske, S. Landowne, H. H. Wolter, T. Tamura, and T. Ugadawa, Phys. Lett. **122B**, 333 (1983).
[39]D. R. Dean, H. Lenske, U. Mosel, and H. H. Wolter, Nucl. Phys. **A427**, 125 (1984).
[40]V. M. Strutinsky, Z. Phys. A **286**, 77 (1978).
[41]A. Y. Abul-Magd and M. H. Simbel, Phys. Lett. **83B**, 27 (1979).
[42]K. M. Hartmann, Z. Phys. A **294**, 65 (1980).
[43]W. Dünnweber and K. M. Hartmann, Phys. Lett. **80B**, 23 (1978).
[44]P. J. Siemens and F. D. Becchetti, Phys. Lett. **42B**, 389 (1972).
[45]D. K. Scott, D. L. Hendrie, L. Kraus, C. F. Maguire, J. Mahoney, Y. Terrien, and K. Yagi, Phys. Rev. Lett. **36**, 226 (1976).
[46]H. J. Krappe, J. R. Nix, and A. J. Sierk, Phys. Rev. C **20**, 992 (1979).
[47]R. W. Hasse, Pramana **11**, 441 (1978).
[48]J. P. Bondorf, M. I. Sobel, and D. Sperber, Phys. Rep. **15**, 83 (1974).
[49]D. H. E. Gross and H. Kalinowski, Phys. Rep. **45**, 175 (1978).
[50]K. T. R. Davies and J. R. Nix, Phys. Rev. C **14**, 1977 (1976).
[51]R. R. Betts and S. B. DiCenzo, Phys. Rev. C **19**, 2070 (1979).
[52]T. M. Cormier, P. Braun-Munzinger, P. M. Cormier, J. W. Harris, and L. L. Lee, Phys. Rev. C **16**, 215 (1977).
[53]A. Gilbert and A. G. W. Cameron, Can. J. Phys. **43**, 1446 (1965).